Crystal Structure of a High-Affinity Variant of Rat α-Parvalbumin†

Yong-Hwan Lee,‡,§ John J. Tanner,*,‡,|| John D. Larson,|| and Michael T. Henzl*,||

Departments of Chemistry and Biochemistry, University of Missouri, Columbia, Missouri 65211

Received April 8, 2004; Revised Manuscript Received June 4, 2004

ABSTRACT: In model peptide systems, Ca^{2+} affinity is maximized in EF-hand motifs containing four carboxylates positioned on the $+x$ and $-x$ and $+z$ and $-z$ axes; introduction of a fifth carboxylate ligand reduces the affinity. However, in rat β-parvalbumin, replacement of Ser-55 with aspartate heightens divalent ion affinity [Henzl, M. T., et al. (1996) *Biochemistry 35*, 5856−5869]. The corresponding α-parvalbumin variant (S55D/E59D) likewise exhibits elevated affinity [Henzl, M. T., et al. (2003) *Anal. Biochem. 319*, 216−233]. To determine whether these mutations produce a variation on the archetypal EF-hand coordination scheme, we have obtained high-resolution X-ray crystallographic data for α S55D/E59D. As anticipated, the aspartyl carboxylate replaces the serine hydroxyl at the $+z$ coordination position. Interestingly, the Asp-59 carboxylate abandons the role it plays as an outer sphere ligand in wild-type rat β, rotating away from the Ca^{2+} and, instead, forming a hydrogen bond with the amide of Glu-62. Superficially, the coordination sphere in the CD site of α S55D/E59D resembles that in the EF site. However, the orientation of the Asp-59 side chain is predicted to stabilize the D-helix, which may contribute to the heightened divalent ion affinity. DSC data indicate that the α S55D/E59D variant retains the capacity to bind 1 equiv of Na^+. Consistent with this finding, when binding measurements are conducted in K^+-containing buffer, divalent ion affinity is markedly higher. In 0.15 M KCl and 0.025 M Hepes-KOH (pH 7.4) at 5 °C, the macroscopic Ca^{2+} binding constants are 1.8×10^{10} and 2.0×10^9 M^{-1}. The corresponding Mg^{2+} binding constants are 2.7×10^6 and 1.2×10^5 M^{-1}.

Ca^{2+} plays a critical role in eukaryotic signal transduction. Transient oscillations in Ca^{2+} levels regulate numerous biological processes, achieving specificity through variations in location, amplitude, duration, and frequency (*1*). These Ca^{2+} signals reflect the coordinated activity of ion channels, ATP-driven Ca^{2+} pumps, and Ca^{2+}-binding proteins. A detailed appreciation of the kinetics and thermodynamics of Ca^{2+}− and Mg^{2+}−protein interactions is therefore essential to our understanding of Ca^{2+} signaling.

EF-hand proteins, the first intracellular Ca^{2+}-binding proteins identified and characterized, participate in myriad Ca^{2+} signaling pathways (*2*−*4*). The "EF-hand" motif consists of a central metal ion-binding loop and short flanking helical elements. Coordination to the bound Ca^{2+} is pseudo-octahedral, and the coordinating residues are typically designated by Cartesian axes. The side chains of loop residues 1, 3, 5, 9, and 12 contribute the $+x$, $+y$, $+z$, $-x$, and $-z$ ligands, respectively. A main chain carbonyl oxygen serves as the $-y$ ligand, and a water molecule commonly occupies the $-x$ position. The $-z$ carboxylate is a bidentate ligand, so the Ca^{2+} is actually heptacoordinate, with pentagonal bipyramidal coordination geometry.

Certain EF-hand proteins serve as Ca^{2+}-dependent regulatory proteins, and others as cytosolic Ca^{2+} buffers. EF-hand metal ion binding properties exhibit corresponding diversity, with the measured Ca^{2+} binding constants spanning 4 orders of magnitude (*5*). After more than two decades of focused inquiry, the underlying physical basis for these variations remains incompletely understood. Although the fundamental determinants of metal ion specificity and affinity are necessarily the same in proteins and small molecule chelators, i.e., size and charge, the protein architecture introduces additional complexity (*6*, *7*).

Parvalbumins are small ($M_r = 12\,000$), vertebrate-specific EF-hand proteins believed to function as Ca^{2+} buffers (*8*, *9*). The parvalbumin (PV)[1] molecule (Figure 1) has been a popular system for investigating structure−affinity correlations. It contains six short helices, labeled A−F. The two Ca^{2+}-binding sites are called the CD and EF sites, in reference to the flanking helical elements. The structure of carp parvalbumin (*10*) established the EF-hand structural paradigm, and in fact, the term EF-hand refers to the parvalbumin EF site.

Roughly 425 million years ago, the PV family diverged into α and β sublineages (*11*, *12*). They are distinguished by isoelectric point (β < 5), C-terminal helix length (generally one residue longer for α), and several lineage-

† This work was supported by NSF Grant MCB0131166 (to M.T.H. and J.T.T.).

* To whom correspondence should be addressed. M.T.H.: telephone, (573) 882-7485; fax, (573) 884-4812; e-mail, henzlm@missouri.edu. J.J.T.: telephone, (573) 884-1280; e-mail, tannerjj@missouri.edu.

‡ Department of Chemistry.

§ Present address: Department of Biological Sciences, Louisiana State University, Baton Rouge, LA 70803.

|| Department of Biochemistry.

[1] Abbreviations: CD site, parvalbumin metal ion-binding site flanked by the C and D helical segments; DSC, differential scanning calorimetry; EDTA, ethylenediaminetetraacetic acid; EF site, parvalbumin metal ion-binding site flanked by the E and F helical segments; EGTA, ethylene glycol bis(β-aminoethyl ether)-*N*,*N*,*N*′,*N*′-tetraacetic acid; Hepes, 4-(2-hydroxyethyl)-1-piperazineethanesulfonic acid; ITC, isothermal titration calorimetry; LB, Luria-Bertani; NLLS, nonlinear least squares; NMR, nuclear magnetic resonance; P_i, phosphate; PV, parvalbumin.

10.1021/bi0492915 CCC: $27.50
Published on Web 07/16/2004

Table 1: Divalent Ion Binding Properties of the Rat α- and β-Parvalbumin Pentacarboxylate Variants

protein	temp (°C)	K_1 (M^{-1})	K_2 (M^{-1})	ΔG_{Ca}[a] (kcal/mol)	$\Delta\Delta G_{Ca}$ (kcal/mol)	K_{1M} (M^{-1})	K_{2M} (M^{-1})	ΔG_{Mg}[a] (kcal/mol)	$\Delta\Delta G_{Mg}$ (kcal/mol)
rat β-PV[b]	25	2.4×10^7	1.4×10^6	−18.4	−	$9.4(0.3) \times 10^3$	$1.6(0.2) \times 10^2$	−8.4	−
β S55D[c]	25	5.3×10^7	1.1×10^7	−20.1	−1.7	4.5×10^4	8.3×10^3	−11.6	−3.2
β G98D[c]	25	2.5×10^8	1.2×10^6	−19.7	−1.3	8.0×10^3	2.6×10^2	−8.6	−0.2
rat α-PV[b]	25	2.5×10^8	6.2×10^7	−22.0	−	3.7×10^4	9.0×10^3	−11.6	−
α S55D[d]	25	2.1×10^8	5.0×10^7	−21.8	0.2	nd[f]	nd[f]	nd[f]	nd[f]
rat α-PV[b]	5	2.6×10^8	6.4×10^7	−20.5	−	1.8×10^4	4.3×10^3	−10.0	−
α S55D/E59D[e]	5	1.9×10^9	2.5×10^8	−24.0	−2.0	2.7×10^5	1.9×10^4	−12.3	−2.3
α G98D[d]	5	1.2×10^9	7.7×10^7	−23.1	−1.1	3.1×10^4	3.3×10^3	−10.2	−0.2

[a] Calculated with the relationship $\Delta G = -RT \ln K_1K_2$. [b] From ref *28*. [c] From ref *26*. [d] From ref *20*. [e] From ref *38*. [f] Not determined.

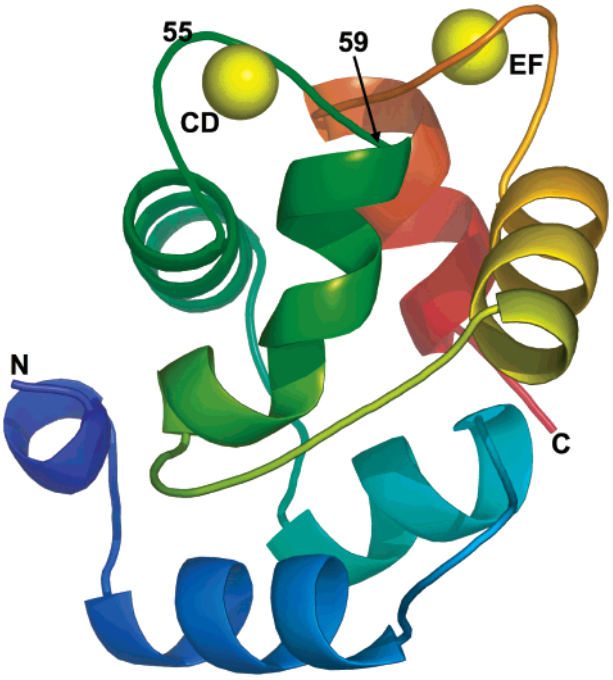

FIGURE 1: Ribbon diagram of the S55D/E59D variant of rat α-parvalbumin, with the approximate locations of residues 55 and 59 indicated.

specific sequence identities (e.g., Cys-18 in β). The mammalian genome encodes one isoform from each lineage (*13*).

Despite 49% sequence identity (*14*, *15*), the rat α- and β-parvalbumins exhibit very different metal ion binding properties. Whereas both metal ion-binding sites in α are high-affinity sites (*16*, *17*), the two sites in β are distinctly nonequivalent. The β EF site is a typical high-affinity site, but the CD site exhibits a low-affinity signature (*18*, *19*). Thus, the mammalian parvalbumins offer an interesting system with which to explore the EF-hand structure−affinity issue.

The parvalbumin CD binding loop, spanning residues 51−62 inclusive, harbors four carboxylate ligands. Besides the main chain carbonyl from residue 57, the ligand array in rat α-parvalbumin includes the side chains from Asp-51 (+*x*), Asp-53 (+*y*), Ser-55 (+*z*), Glu-59 (−*x*), and Glu-62 (−*z*) (Figure 2A). In rat β, Glu-59 is replaced with aspartate. The shorter aspartyl side chain cannot directly coordinate the bound divalent ion. Instead, a water molecule serves as the proximal ligand, and the Asp-59 carboxylate functions as an outer sphere ligand (Figure 2B). The impact of −*x* identity is isoform-dependent. Replacement of Asp-59 with glutamate in rat β produces a very modest increase in Ca^{2+} affinity ($\Delta\Delta G_{Ca} = -0.1$ kcal/mol) (*17*). By contrast, substitution of

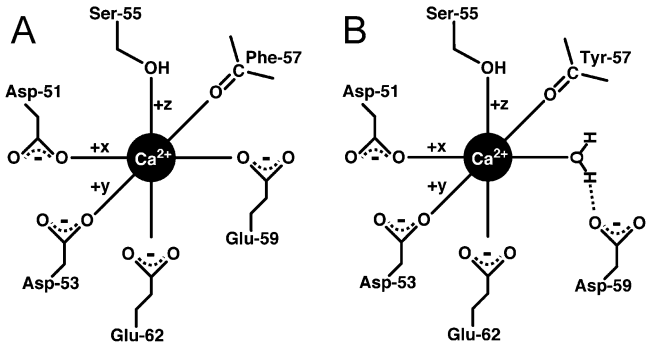

FIGURE 2: Schematic diagrams of the CD sites from rat α-parvalbumin (A) and rat β-parvalbumin (B).

Glu-59 with aspartate in rat α causes a major decrease in Ca^{2+} affinity ($\Delta\Delta G_{Ca} = 1.7$ kcal/mol) (*20*).

Early studies with EF-hand peptide models revealed that Ca^{2+} affinity is maximized in sites containing four carboxylate ligands positioned along the +*x* and −*x* and +*z* and −*z* axes (*21*−*24*). Addition of a fifth carboxylate lowers the binding affinity, presumably because of stronger interligand repulsion (*25*). Unexpectedly, introduction of a fifth carboxylate ligand into either the CD or EF site of rat β produces a significant increase in Ca^{2+} affinity (*26*) (Table 1). Replacement of Ser-55 with aspartate (S55D) in the CD site yields a $\Delta\Delta G_{Ca}$ of −1.7 kcal/mol. Replacement of Gly-98 in the EF site yields a somewhat smaller $\Delta\Delta G_{Ca}$ value (−1.3 kcal/mol).

The corresponding mutations were recently examined in rat α, a more typical parvalbumin isoform (*20*). In contrast to β S55D, the α S55D variant does not exhibit heightened Ca^{2+} affinity (Table 1). Reasoning that this discrepancy reflected the difference in ligation at −*x* (residue 59), we simultaneously mutated Ser-55 and Glu-59 to aspartate, producing a ligand array equivalent to that in β S55D. As anticipated, the resulting α S55D/E59D displays elevated affinity for divalent ions. In Hepes-buffered saline, the combined mutations yield a $\Delta\Delta G_{Ca}$ of −2.0 kcal/mol, with respect to wild-type α. As observed for the β isoform, the magnitude of $\Delta\Delta G_{Ca}$ was smaller for α G98D, approximately −1.1 kcal/mol.

β S55D and α S55D/E59D also display substantial increases in Mg^{2+} affinity, −3.2 and −2.3 kcal/mol, respectively. By contrast, the α and β G98D variants exhibit minor changes in overall Mg^{2+} affinity, with $\Delta\Delta G_{Mg}$ being equal to −0.2 kcal/mol in both cases.

Thermodynamic data on these "pentacarboxylate" variants suggest that the increase in divalent ion affinity can be largely attributed to preferential destabilization of the apoprotein.

However, determining whether these mutations produce any significant variation on the canonical EF-hand coordination theme was a matter of some interest. Although β S55D has thus far proven to be refractory to crystallization, we have obtained crystals of the α homologue, S55D/E59D, that diffract to 2.0 Å. The structure of that variant is described herein.

Rat α binds 1 equiv of Na^+ (*27*), and competition by the monovalent ion significantly attenuates Ca^{2+} affinity (*28*). *A priori*, a loss of Na^+ binding capacity, with the concomitant elimination of solvent cation competition, might have explained the heightened divalent ion affinity of α S55D/E59D. Thus, we have investigated the stoichiometry of Na^+ binding using differential scanning calorimetry. To evaluate the impact of solvent cation identity on divalent ion affinity, we have measured the Ca^{2+} and Mg^{2+} binding constants of α S55D/E59D in K^+-containing solution.

MATERIALS AND METHODS

Expression and Isolation of S55D/E59D. Prior to the start of this project, the rat α coding sequence had been inserted into pLD2, a derivative of pBluescript (Stratagene). The resulting plasmid (rpv-pLD2) supports high-level constitutive expression of wild-type rat α (>50 mg/L of culture). The S55D/E59D variant was obtained by two rounds of mutagenesis, first S55D and then E59D, employing the Transformer site-specific mutagenesis kit (Clontech). The fidelity of the coding sequence in S55D/E55D-pLD2 was confirmed by automated DNA sequencing.

For expression, *Escherichia coli* DH5α cells, harboring S55D/E59D-pLD2, were grown to stationary phase at 37 °C in 1 L cultures of LB broth containing 100 μg of ampicillin. The resulting cell paste was resuspended in 20 mM Hepes-NaOH (pH 7.4) and then lysed by treatment with lysozyme (5.0 mg/g of cell paste) and extrusion from a French pressure cell. The subsequent purification scheme paralleled that described previously for wild-type rat α (*29*). Because the protein lacks tryptophan and tyrosine, the UV absorbance spectrum provides a convenient indicator of purity. If a mass extinction coefficient of 0.5 $(mg/mL)^{-1}$ cm^{-1} at 290 nm for impurities is assumed, the homogeneity of the protein preparations employed for this study exceeded 98%.

X-ray Crystallography. Prior to crystallization, the α S55D/E59D preparation was dialyzed for 48 h against 50 μM Ca^{2+}, and then concentrated to 92 mg/mL. Crystals were grown at 22 °C by vapor diffusion. The reservoir solution contained 30% PEG 4000 and 0.2 M $(NH_4)_2SO_4$. Hanging drops were formed by combining 2 μL of the protein solution with an equal volume of the reservoir solution. For cryogenic data collection, crystals were equilibrated with 30% PEG 4000, 0.2 M $(NH_4)_2SO_4$, and 10% ethylene glycol for 10 min, then captured with a cryoloop, and plunged into liquid nitrogen.

The crystals, belonging to space group $P2_12_12$, had the following unit cell dimensions: $a = 61.5$ Å, $b = 51.6$ Å, and $c = 30.7$ Å. There is one molecule per asymmetric unit. A 2.0 Å data set was collected from a single crystal, employing an R-axis IV detector. X-rays were produced with a Rigaku RU-H3R copper rotating-anode generator equipped with Osmic MaxFlux confocal optics and an X-stream cryogenic system. The data were processed with *HKL* (*30*), and the reflection intensities were converted to amplitudes using the method of French and Wilson (*31*), as implemented in CCP4 (32). The structure was determined by molecular replacement (*33*), employing the 2.0 Å wild-type structure (PDB entry 1RTP) (*34*) as the search model. Refinement and model building were done with CNS (*35*) and O (*36*), respectively. Data collection and processing statistics are given in Table 2.

Table 2: Data Collection and Refinement Statistics

space group	$P2_12_12$
unit cell dimensions (Å)	$a = 61.5$ Å, $b = 51.6$ Å, $c = 30.7$ Å
no. of crystals	1
no. of RPV molecules per asymmetric unit	1
diffraction resolution (Å)	26−2.0 (2.07−2.0)[a]
no. of observations	41537
no. of unique reflections	6981
completeness (%)	99 (98)[a]
mean I/σ_I	15.0 (6.0)[a]
R_{merge}	0.055 (0.14)[a]
no. of protein atoms	829
no. of calcium ions	2
no. of water molecules	129
no. of sulfate ions	1
R_{cryst}	0.181 (0.175)[a]
R_{free}[b]	0.221 (0.247)[a]
rmsd[c]	
bond lengths (Å)	0.009
bond angles (deg)	1.5
dihedral angles (deg)	20.5
improper dihedrals (deg)	0.89
Ramachandran plot[d]	
favored (%)	93.9
allowed (%)	6.1
generous (%)	0.0
disallowed (%)	0.0
average *B*-factors (Å^2)	
protein	18.2
calcium ions	16.9
solvent	26.6

[a] Values for the outer resolution shell of data are given in parentheses. [b] The 10% R_{free} test set. [c] Compared to the Engh and Huber force field (*45*). [d] The Ramachandran plot was generated with PROCHECK (*46*).

Protein Data Bank Entry. The atomic coordinates and structure factors have been deposited in the Protein Data Bank as entry 1S3P.

Differential scanning calorimetry was performed in a modified Nano DSC calorimeter (Calorimetry Sciences Corp.), equipped with cylindrical sample cells (active volume of 0.32 mL). Prior to analysis, samples were dialyzed to equilibrium against the sample buffer of interest, and an aliquot of the dialysis reservoir was used to fill the reference cell. The impact of Na^+ concentration on protein stability was examined in buffers containing 0.005 M sodium phosphate, 0.010 M EDTA (pH 7.4), and NaCl as appropriate. A more limited analysis was also performed using buffers prepared with the corresponding K^+ salts. A scan rate of 1.0°/min was employed for all experiments. Thermodynamic reversibility was demonstrated by repetitive scanning. In every case, an endothermic transition was observed on the rescan, comparable in area to the original. Data analysis was performed with CpCalc version 2.1 (Applied Thermodynamics).

Isothermal Titration Calorimetry. Prior to analysis, residual Ca^{2+} was removed from the protein solution and buffer when they were passed over EDTA-derivatized agarose (*37*) at 4

°C. Because α S55D/E59D binds Ca^{2+} with extremely high affinity in K^+ solution, it was necessary to conduct the Ca^{2+} removal in 0.15 M NaCl and 0.025 M Hepes-NaOH (pH 7.4). The buffer was then replaced with Ca^{2+}-free 0.15 M KCl and 0.025 M Hepes-KOH (pH 7.4) by repetitive rounds of concentration and dilution in an Amicon ultrafiltration cell (YM10 membrane). The residual Ca^{2+} content, measured by flame atomic absorption spectrometry, was less than 0.05 equiv.

The ITC experiments were conducted in a VP-ITC calorimeter (MicroCal, Inc.). Following thermal equilibration, additions of titrant were made, at 200 s intervals, to the 1.41 mL protein samples. Titrations were carried out with Ca^{2+} alone, with Mg^{2+} alone, with Ca^{2+} at several fixed levels of Mg^{2+}, with Ca^{2+} in the presence of EDTA, with Ca^{2+} in the presence of EGTA, and with Mg^{2+} in the presence of EDTA. Following subtraction of the heats of mixing, the results of the experiments were compiled into a master data file. This composite data set was subjected to weighted global nonlinear least-squares (NLLS) analysis, as described elsewhere (*28*, *38*).

Estimation of the α S55D/E59D Na^+ Binding Constants by Monte Carlo Simulation. Synthetic divalent ion binding data were produced, using the apparent binding constants measured in K^+ or Na^+ solution. Estimates of the Na^+ affinity constants for α S55D/E59D were obtained by Monte Carlo analysis, employing a model that includes species M, MX, MX_2, MY, and MXY, where M represents the macromolecule, X represents the relevant divalent ion, and Y represents Na^+. In the presence of Na^+, the extent of divalent ion binding for this system after the *i*th addition, $\bar{X}_i$, is described by the following equation

$$\bar{X}_i = [K_{10}(1 + K_{11}Y_i)X_i + 2K_{20}K_{10}X_i^2]/P \quad (1)$$

where P is the partition function, which is equal to

$$P = 1 + K_{01}Y_i + K_{10}(1 + K_{11}Y_i)X_i + K_{20}K_{10}X_i^2 \quad (2)$$

In eqs 1 and 2, X_i and Y_i are the free divalent ion and Na^+ concentrations, respectively, after the *i*th addition, K_{10} and K_{20} are the true macroscopic association constants for the first and second divalent ion binding events, respectively (i.e., unperturbed by Na^+), K_{01} is the Na^+ binding constant for the apoprotein, and K_{11} is the corresponding constant for the MX species. Because Na^+ was present in such a large excess, X_i was fixed at the total Na^+ concentration.

The divalent ion binding constants measured for α S55D/E59D in K^+ solution provided values for K_{10} and K_{20}. The corresponding analysis of the wild-type protein, reported previously (*28*), yielded starting estimates for the Na^+ binding constants, K_{01} and K_{11}. After calculation of the initial χ^2 value, a new parameter set was generated by incrementing each binding constant by an arbitrary quantity, ΔK. The magnitude of ΔK is equal to the output from a random number generator multiplied by some arbitrary fraction of the initial parameter value. χ^2 was then recalculated. Simulations were performed both with and without minimization, as described elsewhere (*28*). The process was performed until values of K_{01} and K_{11} that brought the calculated binding curve in the presence of Na^+ into agreement with the observed one were identified.

RESULTS

Crystal Structure. Stereoscopic views of the CD sites from the wild-type rat α- and β-parvalbumins are displayed for reference in panels A and B of Figure 3, respectively. As noted previously, the Ca^{2+} coordination chemistry is virtually identical in the two sites, except at the $-x$ position (residue 59). In both wild-type α and β structures, Ser-55 coordinates Ca^{2+} at the $+z$ position, forming a 2.5 Å OG$-Ca^{2+}$ bond (*34*, *39*, *40*). In α, the Glu-59 carboxylate group coordinates the bound ion at $-x$ through a 2.4 Å OE$-Ca^{2+}$ bond. The nonliganding oxygen atom of the Glu-59 carboxylate typically hydrogen bonds to one or more water molecules (Figure 3A). In rat β, a water molecule coordinates at $-x$, making a 2.3 Å bond to the Ca^{2+} ion and a 2.4 Å hydrogen bond to the carboxylate of Asp-59.

The crystal structure of α S55D/E59D was determined to ascertain whether the increase in divalent ion affinity resulting from the double mutation is accompanied by perceptible structural changes in the CD binding site. Ser-55 and Asp-59 are clearly visible in the electron density of the 2.0 Å α S55D/E59D structure (Figure 4). The stereoview of the CD site in α S55D/E59D, displayed in Figure 3C, reveals a significant change in the Ca^{2+} coordination.

Asp-55 coordinates the bound Ca^{2+} in monodentate fashion, with a bond length of 2.5 Å (Figure 3C). At $-x$, a water molecule serves as the ligand (HOH-1, *B*-value = 19 $Å^2$), as in wild-type β, with a $Ca^{2+}-O$ bond length of 2.5 Å. However, in contrast to wild-type β, Asp-59 no longer functions as an outer-sphere ligand in α S55D/E59D. Instead, the carboxylate is directed away from the binding site and is hydrogen-bonded to the backbone amide of Glu-62.

Superficially, the coordination pattern in the mutated CD site of α S55D/E59D resembles that in the wild-type EF site. Besides the invariant backbone carbonyl at $-y$ and the bidentate glutamyl carboxylate at $-z$, aspartyl side chains furnish the $+x$, $+y$, and $+z$ ligands in both cases, and a water molecule provides the $-x$ ligand. Moreover, the $+z$ carboxylate is hydrogen-bonded to the $-x$ water molecule in both the mutant CD site (Figure 3C) and the wild-type EF site.

The structural alterations in the CD site of α S55D/E59D are not confined to the Ca^{2+}-binding ligands. The side chain of Asp-61 has also undergone a major rotation so that it faces away from the Ca^{2+}-binding site (Figure 3C). This structural change has most likely occurred in response to a steric clash generated by the rotation of Asp-59. In this crystal form, the Asp-61 carboxylate interacts with the Asp-10 carboxylate from a symmetry-related molecule (not shown). The O$-$O distance is 2.4 Å, suggesting that the two carboxylates are sharing a proton, a commonly observed interaction in crystal contact regions (*41*).

The structural remodeling of the CD site in S55D/E59D also involves changes in the solvent structure around the CD site. Whereas Ser-55 does not hydrogen bond to solvent in the wild-type CD site (Figure 3A,B), Asp-55 of S55D/E59D interacts with two water molecules (Figure 3C). In addition, the hydrogen bonding between Asp-53 and solvent observed in the wild-type CD site (Figure 3A,B) is absent in S55D/E59D (Figure 3C). Apparently, the presence of aspartate, rather than serine, at position 55 prevents the close approach of water to neighboring Asp-53. Finally, Asp-55 and Asp-59 form a water-mediated interaction in S55D/E59D that is not seen in the wild-type CD site (Figure 3C).

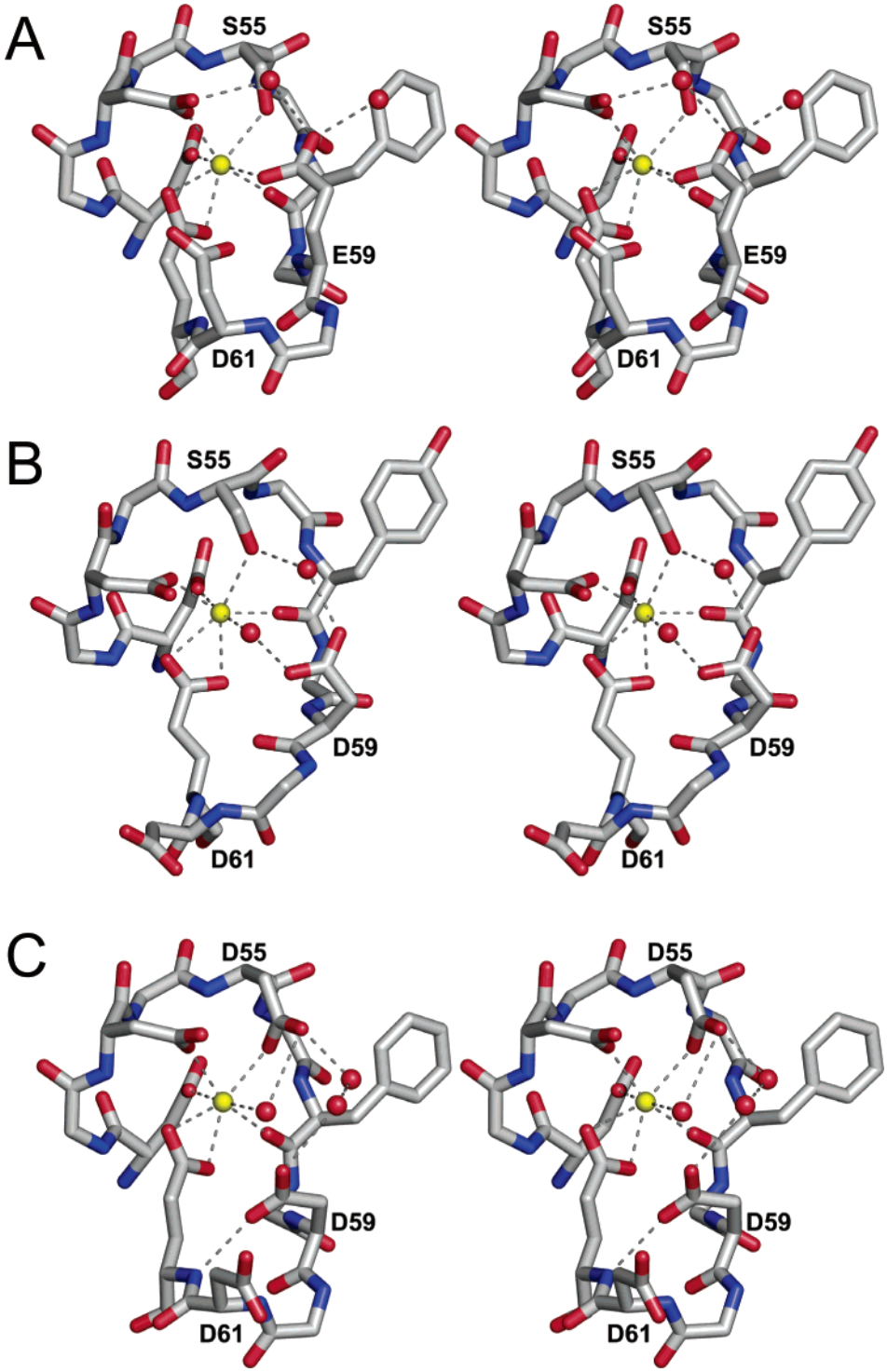

FIGURE 3: (A) Stereoview of the CD site from wild-type rat α-PV (*34*, *40*; PDB entry 1RWY). (B) Stereoview of the CD site from rat *β*-PV (*39*; PDB entry 1RRO). (C) Stereoview of the CD site from rat α S55D/E59D (PDB entry 1S3P). This figure was produced with Pymol (*47*).

Stoichiometry of Na^+ Binding. Wild-type α binds 1 equiv of Na^+ (*27*). The binding event significantly stabilizes the apoprotein and strongly attenuates divalent ion binding (*28*). NMR data suggest that the monovalent ion occupies the vacant CD site in the Ca^{2+}-free protein. Thus, one explanation for the increased Ca^{2+} affinity of the α S55D/E59D variant in Hepes-buffered saline would be a loss of Na^+ binding capacity. To test this possibility, DSC analyses were conducted, as a function of Na^+ concentration, on the Ca^{2+}-free protein. Raw data for a subset of the scans are displayed in Figure 5A; the thermodynamic data, T_m and ΔH_d, are listed in Table 3.

It is evident that, like the wild-type protein, α S55D/E59D is stabilized by Na^+. The transition temperatures have been plotted versus $\ln[Na^+]$ in Figure 5B. The instantaneous slope of this plot, $dT/d(\ln[Na^+])$, is proportional to the stoichiometry of Na^+ binding, as indicated by this equation:

$$\Delta n_{Na^+} = (\Delta H_d/RT_d^2)[dT_d/d(\ln[Na^+])] \qquad (3)$$

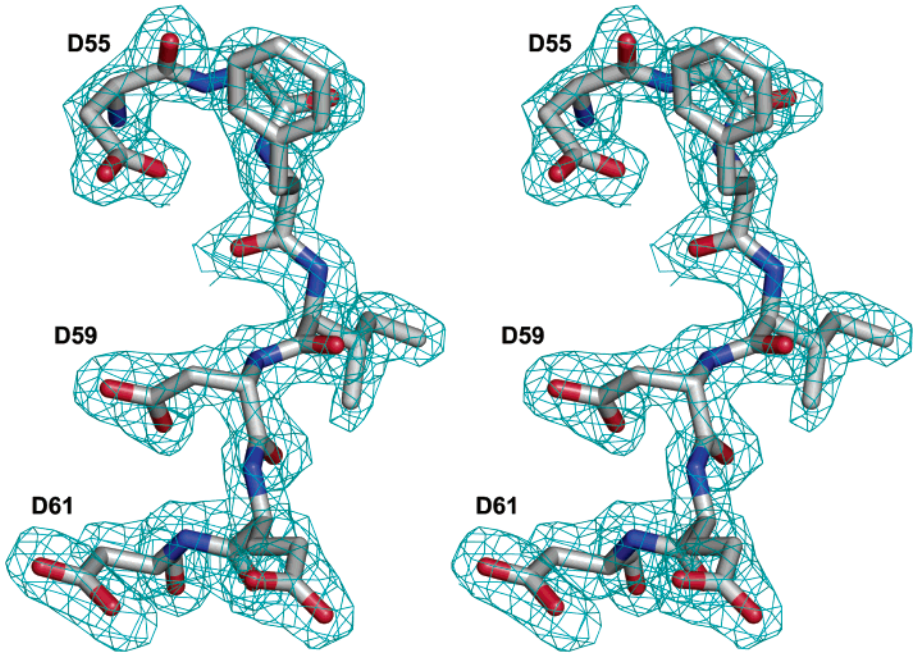

FIGURE 4: $2F_o - F_c$ electron density map (1σ) for the 2.0 Å structure of α S55D/E59D, in the vicinity of Asp-55 and Asp-59.

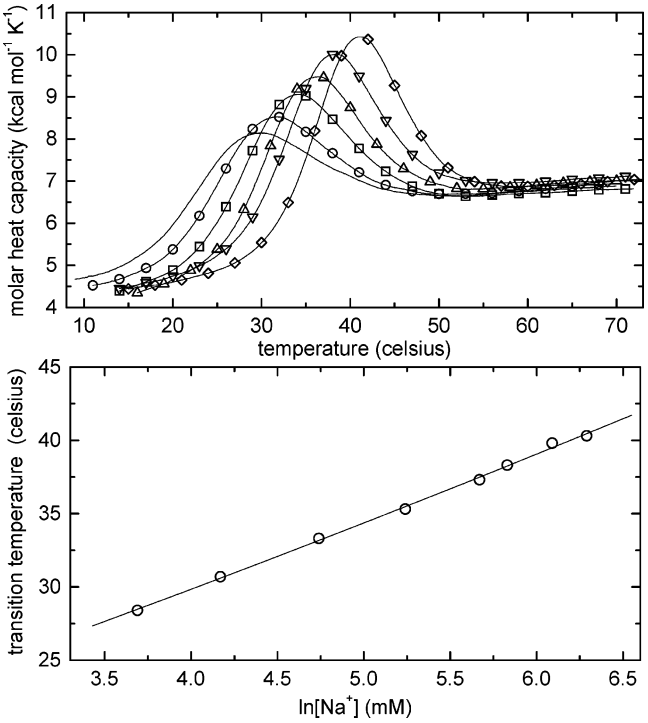

FIGURE 5: Stability of α S55D/E59D as a function of Na^+ concentration. (A) DSC data are shown for experiments conducted at total Na^+ concentrations of 65 (no symbol); 190 (○), 290 (□), 340 (△), 440 (▽), and 540 mM (◇). All of the scans were performed at a protein concentration between 7.0 and 7.4 mg/mL. (B) Stoichiometry of Na^+ binding. The melting temperature is plotted as a function of the natural logarithm of the Na^+ concentration (in millimolar). The solid line indicates the best fit to a second-order polynomial. The slope of the curve when $\ln[Na^+] = 5.29$, corresponding to 200 mM Na^+, was used to calculate the stoichiometry of Na^+ binding, as described in the text.

where ΔH_d is the enthalpy of denaturation, T_d is the melting temperature, and R is the gas constant (*42*). The data in Figure 5B, which show a slight degree of upward curvature, were arbitrarily fit to a second-order polynomial (solid line). At 0.20 M Na^+, the apparent Na^+ stoichiometry is 1.00 ± 0.05, identical to that of wild-type α. Evidently, the combined S55D and E59D mutations do not abolish Na^+ binding ability.

Table 3: T_m and ΔH_d Values for α S55D/E59D as a Function of Na^+ Concentration[a]

[Na^+] (M)	T_m[b] (°C)	ΔH_d[c] (kcal/mol)
0.040	28.4	42
0.065	30.7	46
0.115	33.3	51
0.190	35.3	49
0.290	37.3	55
0.340	38.3	56
0.440	39.8	57
0.540	40.3	57

[a] Samples contained 0.005 mM sodium phosphate, 0.010 M EDTA, and increasing concentrations of NaCl. The pH of the buffer was 7.40 at 25 °C. [b] The estimated uncertainty in the melting temperature is ±0.3°C. [c] The estimated uncertainty in the denaturational enthalpy change is ±5%.

Divalent Ion Binding Affinities of α *S55D/E59D in* K^+*-Containing Solution.* The impact of solvent cation identity on α S55D/E59D divalent ion affinity was examined by conducting binding studies in K^+ solution. Because the affinity of the protein is too high to determine by flow dialysis, an ITC-based approach was employed. The protein was subjected to a battery of titrations, as described in Materials and Methods. The resulting data were compiled into a single data set, which was then analyzed by global NLLS minimization. For ease of analysis, the titrations were conducted at 5 °C. At this temperature, the apoprotein is fully folded in K^+ solution, and the data can be analyzed using a simple two-site binding model. By contrast, at 25 °C, a significant fraction of the protein is unfolded. As a consequence, divalent ion binding is linked to folding, which confounds global analysis with a simple two-site model.

Integrated data for the entire data set are presented in Figure 6B, the solid line indicating the best least-squares fit. The binding parameters thus obtained are presented, along with the corresponding data in Na^+, in Table 4. The divalent

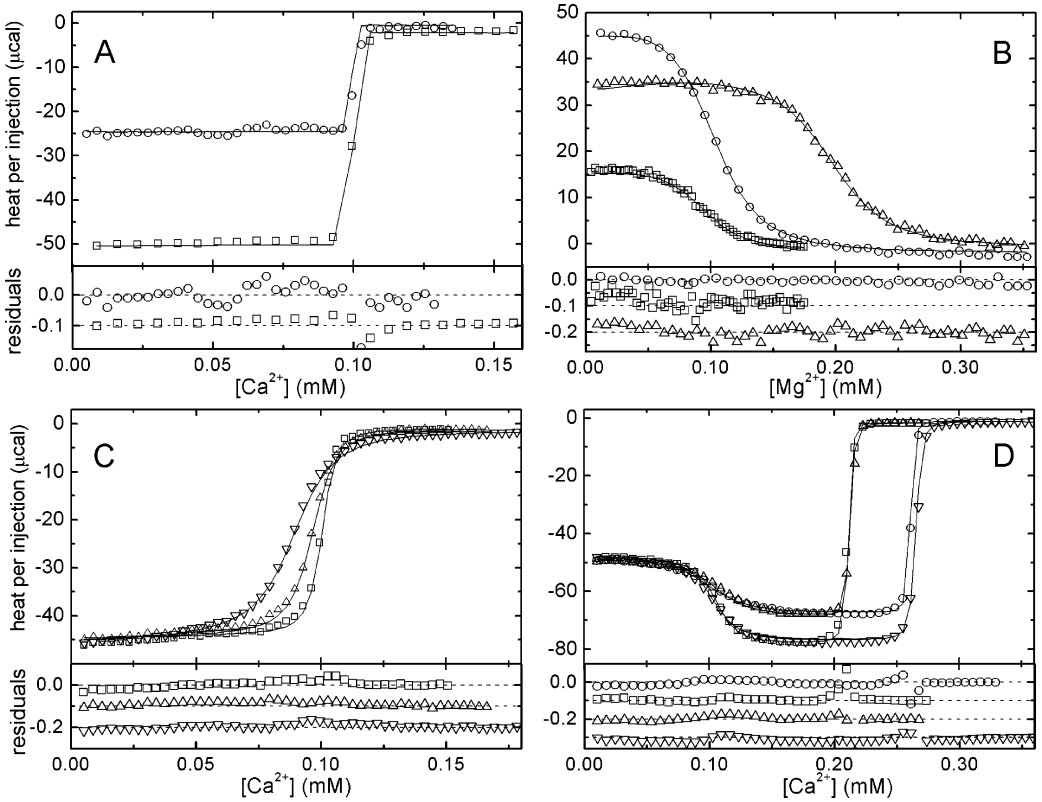

FIGURE 6: ITC analysis of divalent ion binding by α S55D/E59D (55/59D) in K^+-containing buffer: (A) 1.0 mM Ca^{2+} vs 55 μM protein with 5 μL injections (○) and 1.0 mM Ca^{2+} vs 54 μM 55/59D with 10 μL injections (□), (B) 0.93 mM Mg^{2+} vs 55 μM protein with 5 μL injections (□), 1.8 mM Mg^{2+} vs 55 μM 55/59D with 7 μL injections (△), and 1.8 mM Mg^{2+} vs 52 μM 55/59D and 0.17 mM EDTA with 5 μL injections (○), (C) 1.0 mM Ca^{2+} vs 55 μM protein and 1.0 mM Mg^{2+} with 5 μL injections (□), 1.0 mM Ca^{2+} vs 53 μM 55/59D and 3.0 mM Mg^{2+} with 5 μL injections (△), and 1.0 mM Ca^{2+} vs 49 μM 55/59D and 10.0 mM Mg^{2+} with 5 μL injections (▽), and (D) 2.0 mM Ca^{2+} vs 54 μM protein and 0.12 mM EDTA with 7 μL injections (○), 2.0 mM Ca^{2+} vs 52 μM 55/59D and 0.19 mM EDTA with 7 μL injections (□), 2.0 mM Ca^{2+} vs 54 μM 55/59D and 0.12 mM EGTA with 7 μL injections (△), and 2.0 mM Ca^{2+} vs 53 μM 55/59D and 0.19 mM EGTA with 7 μL injections (▽). The residuals for each analysis are displayed beneath the integrated data.

Table 4: Comparison of Wild-Type α and α S55D/E59D Binding Properties in Na^+ and K^+ Solution at 5 °C[a]

		Ca^{2+} binding parameters					Mg^{2+} binding parameters				
protein	cation	K_1	ΔH_1	K_2	ΔH_2	ΔG_{tot}[b]	K_{1M}	ΔH_1	K_{2M}	ΔH_2	ΔG_{tot}[b]
rat α-PV	Na^+	$2.6(0.2) \times 10^8$	−1.4(0.1)	$6.4(0.2) \times 10^7$	−4.0(0.1)	−20.6	$1.8(0.1) \times 10^4$	7.8(0.1)	$4.3(0.2) \times 10^3$	1.6(0.1)	−10.0
	K^+	$2.9(0.4) \times 10^9$	−3.6(0.1)	$6.6(0.8) \times 10^8$	−4.2(0.1)	−23.2	$2.2(0.2) \times 10^5$	4.4(0.1)	$3.7(0.4) \times 10^4$	2.3(0.2)	−12.6
S55D/E59D	Na^+	$1.9(0.3) \times 10^9$	−4.8(0.2)	$2.9(0.5) \times 10^8$	−4.4(0.2)	−22.5	$2.6(0.4) \times 10^5$	3.1(0.1)	$2.0(0.3) \times 10^4$	4.3(0.1)	−12.3
	K^+	$1.8(0.4) \times 10^{10}$	−4.6(0.2)	$2.0(0.4) \times 10^9$	−4.6(0.2)	−24.9	$2.7(0.6) \times 10^6$	3.5(0.1)	$1.2(0.2) \times 10^5$	3.9(0.1)	−14.6

[a] Macroscopic binding constants are expressed as inverse molar, and energies as kilocalories per mole. Uncertainties (68% confidence intervals) are displayed in parentheses. Data for rat α in Na^+ and K^+ are from ref *28*. Data for α S55D/E59D in Na^+ are from ref *38*. [b] $\Delta G_{tot} = -RT \ln K_1K_2$.

ion affinity of α S55D/E59D is extremely high in K^+ solution, with the first Ca^{2+} binding constant exceeding 10^{10} M^{-1} and the first Mg^{2+} binding constant exceeding 10^6 M^{-1}.

The overall ΔG values for the binding of Ca^{2+} and Mg^{2+} to wild-type α are 2.6 kcal/mol more favorable in K^+ solution than in Na^+. Similar behavior is observed for the S55D/E59D variant. The $\Delta\Delta G$ values for Ca^{2+} and Mg^{2+} binding are −2.4 and −2.3 kcal/mol, respectively.

DISCUSSION

Ca^{2+} Coordination in the α S55D/E59D CD Site. Simultaneous replacement of Ser-55 and Glu-59 with aspartate residues in rat α should produce a ligand constellation equivalent to that in β S55D. In addition to the invariant main chain carbonyl at $-y$ and bidentate glutamyl carboxylate at $-z$, the CD site ligand array in wild-type rat β-PV incorporates aspartate at $+x$ and $+y$ and a serine hydroxyl at $+z$. Although a water molecule serves as the proximal ligand at $-x$, the carboxylate of Asp-59, strongly hydrogen-bonded to the water, plays an indirect role in Ca^{2+} ligation at this position. It was anticipated that mutation of Ser-55 to aspartate would result in substitution of the Asp-55 carboxylate for the serine hydroxyl at the $+z$ position. The consequences of the mutation for coordination at $-x$ were less certain. Would the liganding water molecule remain? If so, would the Asp-59 carboxylate remain hydrogen-bonded to it? This structural analysis was intended to address these questions.

As expected, the carboxylate of Asp-55 replaces the serine hydroxyl at $+z$, and the water molecule is retained at $-x$. Interestingly, however, Asp-59 reacts to the introduction of Asp-55 by withdrawing completely from the coordination sphere. The carboxylate rotates approximately 130°,

away from the Ca^{2+} and bound water molecule, assuming a position adjacent to the amide group of Glu-62.

With aspartyl ligands at $+x$, $+y$, and $+z$ and a water molecule at $-x$, the α S55D/E59D CD site, and the β S55D CD site, by inference, strongly resembles a wild-type EF site. The sole difference is that glycine, rather than the nonparticipatory aspartate, occupies the $-x$ position in the EF site. However, the consequences of introducing the EF site ligand array into the CD site have been examined in both rat β (*43*) and rat α (*20*). In neither case does the ligand remodeling increase the divalent ion affinity of the CD site. Thus, although Asp-59 in α S55D/E59D does not actively participate in metal ion binding, it nevertheless has a major impact on the free energies of Ca^{2+} and Mg^{2+} binding.

There are at least two factors to consider. First, placement of the Asp-59 carboxylate in α S55S/E59D proximal to the Glu-62 amide should stabilize the D helix dipole and, hence, the Ca^{2+}-bound form of the protein. A more important consideration, and one that cannot be discerned by inspection of the Ca^{2+}-bound structure, pertains to the Ca^{2+}-free protein. Specifically, DSC analyses indicate that the apo forms of the pentacarboxylate variants have significantly reduced conformational stability. This destabilization contributes significantly to the ΔG for divalent ion binding. For example, the S55D mutation in wild-type β increases Ca^{2+} affinity by 1.7 kcal/mol. Of that amount, 1.0 kcal/mol can be attributed to destabilization of the apoprotein (*26*). The S55D mutation in α E59D actually increases Ca^{2+} affinity by a full 3.7 kcal/mol, 3.0 kcal/mol of which can be attributed to apoprotein destabilization (*20*). Presumably, the remaining 0.7 kcal/mol in each case reflects the helix capping effect of Asp-59 (*44*).

More than two decades ago, on the basis of studies with EF-hand peptide models, Reid and Hodges proposed the acid pair hypothesis (*21*). The major tenet of their hypothesis is that Ca^{2+} affinity is maximal in an EF-hand motif containing four carboxylates paired on the $+x$ and $-x$ and $+z$ and $-z$ axes. According to this premise, addition of a fifth carboxylate should reduce metal ion affinity, because of stronger interligand repulsion. Our finding that the S55D and G98D mutations, both of which add a potential fifth carboxylate to the ligand array, actually heighten divalent ion affinity (*20*, *26*) was seen as a contradiction of the acid pair hypothesis. The structure of α S55D/E59D provides welcome insight into this issue.

In fact, to the extent that the behavior of α S55D/E59D is general, the acid pair hypothesis appears to be vindicated. The CD site exhibits a clear preference for just four carboxylates. Although replacement of Ser-55 with aspartate introduces an additional carboxylate at $+z$, it causes displacement of the indirectly coordinated carboxylate of Asp-59. Thus, the net number of liganding carboxylates remains unchanged at four. The increased affinity results not from the insertion of an additional anionic ligand. Rather, it results from destabilization of the apoprotein (most likely a consequence of stronger electrostatic repulsion) and, apparently, stabilization of the D helix dipole.

α *S55D/E59D Retains the Capacity To Bind* Na^+. The conclusion that α S55D/E59D exhibits increased affinity for Ca^{2+} and Mg^{2+} was based on binding measurements in Na^+-containing buffer (*38*). Ca^{2+}-free rat α-PV binds 1 equiv of Na^+, and the bound Na^+ apparently occupies one of the vacant EF-hand binding loops (*27*, *28*). Moreover, competition by the monovalent ion has a major impact on rat α divalent ion affinity. Thus, there was a significant possibility that the heightened affinity displayed by α S55D/E59D was merely the reflection of a reduced capacity to interact with Na^+ and, hence, weaker competition by the monovalent ion.

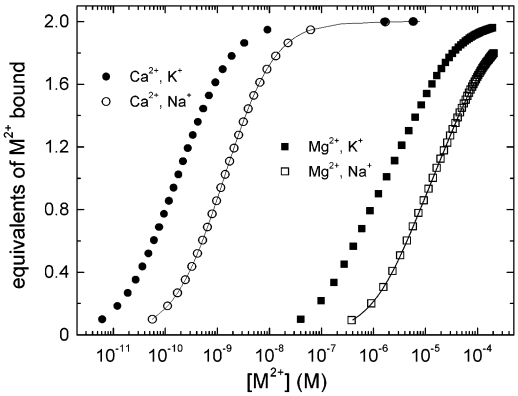

FIGURE 7: Estimation of the Na^+ affinity of α S55D/E59D by Monte Carlo simulation of divalent ion binding data acquired in K^+ and Na^+ buffer. Data sets were synthesized for the binding of Ca^{2+} in K^+ (●) or Na^+ (○) solution and for the binding of Mg^{2+} in K^+ (■) or Na^+ (□) solution, using the apparent binding constants determined by ITC under the various solution conditions.

To test this hypothesis, the stability of Ca^{2+}-free α S55D/E59D was examined by DSC, as a function of Na^+ concentration. As previously observed for wild-type α, the melting temperature depends strongly on the Na^+ concentration. Increasing the solvent cation concentration from 40 to 540 mM increased the T_m from 28.4 to 40.3 °C. By contrast, K^+ has a very minor impact on stability. Whereas the T_m is 37.3 °C in the presence of 290 mM Na^+, it is just 27.3 °C at a comparable K^+ concentration (data not shown). The apparent stoichiometry of Na^+ binding, extracted from a plot of melting temperature versus ln[Na^+], is 1.0, identical to the wild-type value.

As observed for wild-type α, solvent cation identity strongly impacts α S55D/E59D behavior. Replacing Na^+ with K^+ produces a major increase in divalent ion affinity. In K^+ solution, K_1 and K_2, the macroscopic constants governing Ca^{2+} binding, are increased by factors of 10 and 8 to 1.9×10^{10} and 2.3×10^9 M^{-1}, respectively. The corresponding Mg^{2+} constants increase by factors of 11 and 5.5 to 2.8×10^6 and 1.1×10^5 M^{-1}, respectively. Thus, the Ca^{2+} affinity increases by 2.4 kcal/mol when K^+ replaces Na^+ as the solvent cation, and the Mg^{2+} affinity increases by 2.3 kcal/mol.

The attenuation of divalent ion affinity observed in Na^+-containing solution can be used to extract estimates of the Na^+ binding constants, employing a model that explicitly considers the Na^+ binding event. Monte Carlo simulations were conducted as described in Materials and Methods. The Ca^{2+} binding constants measured in Na^+ solution are consistent with estimates for K_{01} and K_{11} of 340 and 36 M^{-1}, respectively, where K_{01} and K_{11} represent the monovalent ion binding constants for the apo and single Ca^{2+}-bound species, respectively (Figure 7). The Mg^{2+} constants measured in the two buffer systems yield similar values of 330 and 29 M^{-1}, respectively. The corresponding values for the binding of Na^+ to wild-type α are 650 and 50 M^{-1}, respectively, suggesting that the combined S55D and E59D

mutations have reduced the affinity for Na^+ by a factor of approximately 2. The estimated Na^+ dissociation constant for the apo form of α S55D/E59D is 2.9 mM.

Under intracellular conditions, with K^+ as the predominant solvent cation and an intracellular Na^+ constant of roughly 10 mM, the Ca^{2+} and Mg^{2+} binding constants will be nearly 1 order of magnitude larger than those for the wild-type protein. A binding constant is, of course, the ratio of the rate constants for ligand association (k_{on}) and dissociation (k_{off}). Thus, the increased divalent ion affinity of α S55D/E59D may reflect a substantial reduction in the k_{off} values. This scenario, if supported by kinetic data, could explain the apparent absence of the pentacarboxylate binding site in nature. Specifically, a reduced rate of divalent ion release might hinder $Ca^{2+}-Mg^{2+}$ exchange and prevent effective Ca^{2+} buffering.

REFERENCES

1. Berridge, M. J. (1997) Elementary and global aspects of calcium signaling, *J. Physiol. 499*, 291−306.
2. Kretsinger, R. H. (1980) Structure and evolution of calcium modulated proteins, *CRC Crit. Rev. Biochem. 8*, 115−164.
3. Kawasaki, H., and Kretsinger, R. H. (1994) Calcium-binding proteins 1: EF-hands, *Protein Profile 1*, 343−517.
4. Celio, M. R., Pauls, T., and Schwaller, B. (1996) *Guidebook to the Calcium-Binding Proteins*, Oxford University Press, New York.
5. Seamon, K. B., and Kretsinger, R. H. (1983) Calcium-modulated proteins, in *Calcium in Biology* (Spiro, T. G., Ed.) pp 3−51, John Wiley and Sons, New York.
6. Falke, J. J., Drake, S. K., Hazard, A. L., and Peersen, O. B. (1994) Molecular tuning of ion binding to calcium signaling proteins, *Q. Rev. Biophys. 27*, 219−290.
7. Linse, S., and Forsen, S. (1995) Determinants that govern high-affinity calcium binding, *Adv. Second Messenger Phosphoprotein Res. 30*, 89−151.
8. Wnuk, W., Cox, J. A., and Stein, E. A. (1982) Parvalbumins and other soluble high-affinity calcium-binding proteins from muscle, in *Calcium and Cell Function* (Cheung, W. Y., Ed.) Vol. 2, pp 243−278, Academic Press, New York.
9. Pauls, T. L., Cox, J. A., and Berchtold, M. W. (1996) The Ca^{2+}-binding proteins parvalbumin and oncomodulin and their genes: new structural and functional findings, *Biochim. Biophys. Acta 1306*, 39−54.
10. Kretsinger, R. H., and Nockolds, C. E. (1973) Carp muscle calcium-binding protein. II. Structure determination and general description, *J. Biol. Chem. 248*, 3313−3326.
11. Goodman, M., and Pechére, J.-F. (1977) The evolution of muscular parvalbumins investigated by the maximum parsimony method, *J. Mol. Evol. 9*, 131−158.
12. Nakayama, S., Moncrief, N. D., and Kretsinger, R. H. (1992) Evolution of EF-hand calcium-modulated proteins. II. Domains of several subfamilies have diverse evolutionary histories, *J. Mol. Evol. 34*, 416−448.
13. Fohr, U. G., Weber, B. R., Muntener, M., Staudenmann, W., Hughes, G. J., Frutiger, S., Banville, D., Schafer, B. W., and Heizmann, C. W. (1993) Human alpha and beta parvalbumins. Structure and tissue-specific expression, *Eur. J. Biochem. 215*, 719−727.
14. Epstein, P., Means, A. R., and Berchtold, M. W. (1986) Isolation of a rat parvalbumin gene and full length cDNA, *J. Biol. Chem. 261*, 5886−5891.
15. Gillen, M. F., Banville, D., Rutledge, R. G., Narang, S., Seligy, V. L., Whitfield, J. F., and MacManus, J. P. (1987) A complete complementary DNA for the oncodevelopmental calcium-binding protein, oncomodulin, *J. Biol. Chem. 262*, 5308−5312.
16. Pauls, T. L., Durussel, I., Cox, J. A., Clark, I. D., Szabo, A. G., Gagne, S. M., Sykes, B. D., and Berchtold, M. W. (1993) Metal binding properties of recombinant rat parvalbumin wild-type and F102W mutant, *J. Biol. Chem. 268*, 20897−20903.
17. Eberhard, M., and Erne, P. (1994) Calcium and magnesium binding to rat parvalbumin, *Eur. J. Biochem. 222*, 21−26.
18. Hapak, R. C., Lammers, P. J., Palmisano, W. A., Birnbaum, E. R., and Henzl, M. T. (1989), Site-specific substitution of glutamate for aspartate at position 59 of rat oncomodulin, *J. Biol. Chem. 264*, 18751−18760.
19. Cox, J. A., Milos, M., and MacManus, J. P. (1990) Calcium- and magnesium-binding properties of oncomodulin, *J. Biol. Chem. 265*, 6633−6637.
20. Henzl, M. T., Agah, S., and Larson, J. D. (2004) Rat α- and β-Parvalbumins: A Comparison of their Penta-carboxylate and Site-interconversion Variants, *Biochemistry* (in press).
21. Reid, R. E., and Hodges, R. S. (1980) Co-operativity and calcium/magnesium binding to troponin C and muscle calcium binding parvalbumin: an hypothesis, *J. Theor. Biol. 84*, 401−444.
22. Reid, R. E. (1990) Synthetic fragments of calmodulin calcium-binding site III. A test of the acid pair hypothesis, *J. Biol. Chem. 265*, 5971−5976.
23. Procyshyn, R. M., and Reid, R. E. (1994) A structure/activity of calcium affinity and selectivity using a synthetic peptide model of the helix-loop-helix calcium-binding motif, *J. Biol. Chem. 269*, 1641−1647.
24. Procyshyn, R. M., and Reid, R. E. (1994) An examination of glutamic acid in the $-x$ chelating position of the helix-loop-helix calcium binding motif, *Arch. Biochem. Biophys. 311*, 425−429.
25. Marsden, B. J., Hodges, R. S., and Sykes, B. D. (1988) ^{1}H NMR studies of synthetic peptide analogues of calcium-binding site III of rabbit skeletal troponin C: effect on the lanthanum affinity of the interchange of aspartic acid and asparagines residues at the metal ion coordinating positions, *Biochemistry 27*, 4198−4206.
26. Henzl, M. T., Hapak, R. C., and Goodpasture, E. A. (1996) Introduction of fifth carboxylate ligand heightens affinity of the oncomodulin CD and EF sites for Ca^{2+}, *Biochemistry 35*, 5856−5869.
27. Henzl, M. T., Larson, J. D., and Agah, S. (2000), Influence of monovalent cations on rat α- and β-parvalbumin stabilities, *Biochemistry 39*, 5859−5867.
28. Henzl, M. T., Larson, J. D., and Agah, S. (2004) Influence of monovalent cation identity on parvalbumin divalent ion-binding properties, *Biochemistry 43*, 2747−2763.
29. Henzl, M. T., and Graham, J. S. (1999) Conformational stabilities of the rat α- and β-parvalbumins, *FEBS Lett. 442*, 241−245.
30. Otwinowski, Z., and Minor, W. (1997) Processing of X-ray diffraction data collected in oscillation mode, *Methods Enzymol. 276*, 307−326.
31. French, G. S., and Wilson, K. S. (1978) On the treatment of negative intensity observations, *Acta Crystallogr. A34*, 517−525.
32. Collaborative Computational Project No. 4 (1994) The CCP4 suite: programs for protein crystallography, *Acta Crystallogr. D50*, 760−763.
33. Vagin, A., and Teplyakov, A. (1997) MOLREP: an automated program for molecular replacement, *J. Appl. Crystallogr. 30*, 1022−1025.
34. McPhalen, C. A., Sielecki, A. R., Santarsiero, B. D., and James, M. N. G. (1994) Refined crystal structure of rat parvalbumin, a mammalian α-lineage parvalbumin, at 2.0 Å resolution, *J. Mol. Biol. 235*, 718−732.
35. Brünger, A. T., Adams, P. D., Clore, G. M., DeLano, W. L., Gros, P., Grosse-Kunstleve, R. W., Jiang, J. S., Kuszewski, J., Nilges, M., Pannu, N. S., Read, R. J., Rice, L. M., Simonson, T., and Warren, G. L. (1998) Crystallography and NMR system: a new software suite for macromolecular structure determination, *Acta Crystallogr. D54*, 905−921.
36. Jones, T. A., Zou, J.-Y., Cowan, S. W., and Kjeldgaard, M. (1991) Improved methods for building protein models in electron density maps and the location of errors in these models, *Acta Crystallogr. A47*, 110−119.
37. Henzl, M. T., Agah, S., and Larson, J. D. (2003) Characterization of the metal ion-binding domains from rat α- and β-parvalbumins, *Biochemistry 42*, 3594−3607.
38. Henzl, M. T., Larson, J. D., and Agah, S. (2003) Estimation of parvalbumin Ca^{2+}- and Mg^{2+}-binding constants by global least squares analysis of isothermal titration calorimetry data, *Anal. Biochem. 319*, 216−233.
39. Ahmed, F. R., Rose, D. R., Evans, S. V., Pippy, M. E., and To, R. (1993) Refinement of recombinant oncomodulin at 1.30 Å resolution, *J. Mol. Biol. 230*, 1216−1224.

40. Bottoms, C. A., Schuermann, J. P., Agah, S., Henzl, M. T., and Tanner, J. J. (2004) Crystal structure of rat α-parvalbumin at 1.05 Å resolution, *Protein Sci.* (in press).
41. Flocco, M. M., and Mowbray, S. L. (1995) Strange bedfellows: interactions between acidic side chains in proteins, *J. Mol. Biol. 254*, 96−105.
42. Alberty, R. A. (1969) Maxwell relations for thermodynamic quantities of biochemical reactions, *J. Am. Chem. Soc. 91*, 3899−3903.
43. Henzl, M. T., Hapak, R. C., and Likos, J. J. (1998) Interconversion of the ligand arrays in the CD and EF sites of oncomodulin. Influence on Ca^{2+}-binding affinity, *Biochemistry 37*, 9101−9111.
44. Richardson, J. S., and Richardson, D. C. (1988) Amino acid preferences for specific locations at the ends of alpha helices, *Science 240*, 1648−1652.
45. Engh, R. A., and Huber, R. (1991) Accurate bond and angle parameters for X-ray protein structure refinement, *Acta Crystallogr. A47*, 392−400.
46. Laskowski, R. A., MacArthur, M. W., Moss, D. S., and Thornton, J. M. (1993) PROCHECK: a program to check the stereochemical quality of protein structures, *J. Appl. Crystallogr. 26*, 283−291.
47. DeLano, W. L. (2002) The PyMOL molecular graphics system. http://www.pymol.org.

BI0492915